Journal of Sound and Vibration 326 (2009) 75–87

Contents lists available at ScienceDirect

Journal of Sound and Vibration

journal homepage: www.elsevier.com/locate/jsvi

Robust control of electrodynamic shaker with 2dof control using H_∞ filter

Y. Uchiyama [a,*], M. Mukai [b], M. Fujita [c]

[a] IMV CORPORATION, Nishiyodogawa-ku, Osaka 555-0011, Japan
[b] Department of Electrical and Electronic Systems Engineering, Graduate School of Information Science and Electrical Engineering, Kyushu University, Nishi-ku, Fukuoka 819-0395, Japan
[c] Department of Mechanical and Control Engineering, Tokyo Institute of Technology, Meguro-ku, Tokyo 152-8550, Japan

ARTICLE INFO

Article history:
Received 27 September 2008
Received in revised form
21 February 2009
Accepted 19 April 2009
Handling Editor: J. Lam
Available online 27 May 2009

ABSTRACT

This paper presents the application of a two-degree-of-freedom (2dof) control of an electrodynamic shaker that is not permitted to employ the iteration control method. In order to improve the control performance, an adaptive filter is added to the 2dof controller using μ-synthesis in the feedback controller. The uncertainty of the controlled plant is taken into account and the adaptive filter based on the H_∞ filtering problem is employed. In comparison to using a general 2dof controller and adaptive filter, the system remains robust against the uncertainty. A good performance for the controller is achieved in experiments by using actual equipment with the nonlinear characteristics that exists in the secondary path.

1. Introduction

Shaking systems, which have become more accurate in replicating actual situations, are used in vibration-proof tests for a wide variety of applications, such as civil and architectural engineering, and the automotive industry. Using electrodynamic shakers has several advantages, such as good linearity and a wide-frequency response; they also allow for more accurate vibration tests when they comprise the shaking system. The controller for a shaking system is required to provide not only stability but also a good replication of the given reference waveform. In order to obtain a good tracking performance, the controller primarily has to compensate for the nonlinear characteristic of the controlled system and the influence of the test piece. Conventional controllers employ the open-loop method that compensates iteratively through repetitive excitations. However, if the test piece is fragile, the specimen breaks before it is subjected to the desired excitation level; this is because of the damage caused to the specimen after each iteration. Therefore, the iterative control method cannot be used in this case. Because of this, finding new methods that do not employ iteration control has recently attracted attention. These methods are studied by combining an actual vibration test with a computer simulation [1], as they require shakers to be controlled in real-time without delaying the computer simulation.

There are several impressive control applications for electrodynamic shakers, such as an adaptive inverse control for shock testing [2] and implementations of current and acceleration controllers [3]. However, since the test applications are different from this requirement, the approaches are not appropriate in this case. In contrast, several features can and have been adapted from electrohydraulic shakers. For example, the minimal control synthesis method, one of the model reference adaptive control methods, has successfully been applied [4], and the real-time compensator of a reaction force

* Corresponding author. Tel.: +81 6 6478 2588; fax: +81 6 6478 2587.
E-mail address: uchiyama@imv.co.jp (Y. Uchiyama).

0022-460X/$ - see front matter © 2009 Elsevier Ltd. All rights reserved.
doi:10.1016/j.jsv.2009.04.024

has cancelled out its influence [5]. However, these control methods do not explicitly consider uncertainties such as the influence of the test piece. Concerning the electrodynamic shaker, its influence generally becomes prominent in comparison with the electrohydraulic shaker. Therefore, explicitly taking into account the uncertainty is necessary. There are many successful cases of applications with robust vibration control, such as controls for active suspensions [6], dual-stage actuators in a hard disk drive [7], and steering wheel vibration simulators [8].

On the other hand, an improvement in control performance is also required, such as when considering the stability of a plant. Since the designs for system stability and control performance can be treated independently, a two-degree-of-freedom (2dof) controller is often used to achieve this advantage. There have been several studies where elements of adaptive control were employed in the feedforward block to improve the control performance when accurate modelling was difficult, with good results [9,10]. By using the adaptive filter on the control structure of the 2dof controller, the filter only has to compensate for the difference between the nominal model and the actual plant beyond the controllable band of the feedback controller. In a previous study by the current authors, the 2dof controller for an electrodynamic shaking system that used μ-synthesis in the feedback control and an adaptive filter was applied [11].

In applications of the adaptive filter, the transfer characteristic for the "secondary path", which refers to the path from the adaptive filter output to the control point, is generally known. For expedience, the transfer characteristic for the secondary pass in this case is generally assumed to be known as well. However, uncertainties caused by nonlinear characteristics and the influence of the test piece exist in the actual secondary path. Therefore, the adaptive filter needs to be able to take into account these uncertainties. In order to compensate for the influence of this problem, several good studies have proposed methods such as adaptive active noise systems with online secondary path modelling [12,13] and active noise control algorithms without secondary path identification [14,15].

In this paper, an adaptive filter based on the H_∞ filter [16] is used. This method has been applied to active noise control [16] and adaptive equalizers over wireless channels [17] and achieves a better performance compared with the general filtered-X LMS method. As the uncertainty existing in the secondary path can be assumed to be a disturbance, and solving the H_∞ filtering problem yields an optimal solution under the assumption of the worst case scenario for unknown disturbances, the control performance improves for a controlled plant where uncertainties exist. In the proposed controller constitution, uncertainties inevitably exist in the secondary path, which contains the controlled system. Therefore, this adaptive filter is a suitable method to constitute the controller.

For the primary evaluation of the 2dof controller with the adaptive method mentioned above in this paper, a single-axis compact shaker is used; the control performance is investigated through an excitation experiment. The rest of the paper is organized as follows. Section 2 introduces a mathematical model and an uncertainty weighting function for the system; Section 3 presents a feedback controller designed by μ-synthesis and a 2dof controller; Section 4 describes the application of an adaptive filter based on the H_∞ filter; Section 5 provides some experimental results; and finally, the paper is summarized in Section 6.

2. Model for an electrodynamic shaker

The outline of the electrodynamic shaker is explained here. A nominal model and an uncertainty weighting function for the system are also introduced.

2.1. Nominal model

The electrodynamic shaker shown in Fig. 1 is based upon the principle that an electrodynamic force is generated in proportion to an electric current applied to the coil existing in the magnetic field. To perform the vibration test at a lower frequency band, the armature displacement of the shaker is selected as a controlled quantity and is measured using a laser displacement sensor. The simplified model of the electrodynamic shaker is as a vibration system with a single degree of freedom, as shown in Fig. 1. By assuming the magnetic flux density to be constant, the drive coil can be represented as a linear equivalent circuit; this in turn allows for a mathematical model of the electrodynamic shaker

$$m\ddot{y}_s = BlI_1 - C_d\dot{y}_s - K_d y_s, \tag{1}$$

$$L_1\dot{I}_1 = -Bl\dot{y}_s - R_1 I_1 + G_a u_s. \tag{2}$$

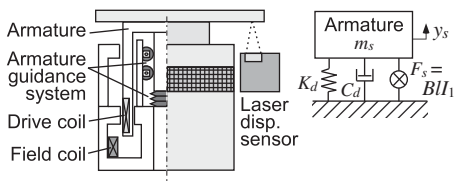

Fig. 1. Overview of an electrodynamic shaker and schematic diagram of the shaker model.

Table 1
Parameters for the electrodynamic shaker and its perturbed region.

Symbol	Parameter	Perturbed region (%)
m	Armature mass	−30 to 30
K_d	Stiffness coefficient of suspension	−40 to 80
C_d	Damping coefficient of suspension	−30 to 30
L_1	Inductance of drive coil	−30 to 30
R_1	Resistance of drive coil	−4 to 18
B	Magnetic flux density	−20 to 20
l	Length of drive coil	
G_a	Amplifier gain	
u_s	Input voltage to amplifier	
y_s	Armature displacement	
I_1	Current of drive coil	

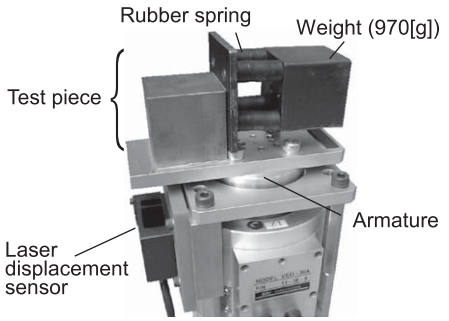

Fig. 2. Overview of the electrodynamic shaker with the test piece.

The parameters and variables are listed in Table 1. By rewriting Eqs. (1) and (2), the transfer function from the input voltage u_s of the amplifier to the displacement y_s of the armature is shown as follows:

$$G_s' = \frac{BlG_a}{mL_1s^3 + (mR_1 + C_dL_1)s^2 + (K_dL_1 + C_dR_1 + (Bl)^2)s + K_dR_1}. \tag{3}$$

The characteristic of a noise-cut filter and the AC coupling of the amplifier are added to the transfer function G_s', resulting model is defined as the nominal model G_s. A second-order low pass Butterworth filter is used for the noise cut, and a first-order high pass filter is used for the AC coupling.

2.2. Modelling uncertainty

The control performance is evaluated by using the experimental shaker shown in Fig. 2. Similar to an actual scenario, it is considered that a resonant specimen is applied and a 970 g specimen is supported by a rubber spring as shown in Fig. 2. The first-order resonant frequency of the specimen is approximately 13 Hz. Due to the influence of the resonance, a peak notch appears in the transfer characteristic of the shaker close to the resonant frequency. This influence is considered as an uncertainty because a stable excitation is performed irrespective of the characteristics of a specimen. However, in this study, a small experimental shaker is used. Thus, the kind of specimen that can be used is restricted, and it was difficult to obtain a nonlinear characteristic of the shaker merely through the influence of the specimen.

Furthermore, in order to add to the nonlinear characteristics of the shaker, friction is generated by increasing the clamping pressure of the suspension system. To investigate the influence of the friction, the transfer function of the plant is measured by using input signals of white noise to monitor rms values that differ correspondingly. The results are shown in Fig. 3, with the solid blue lines representing the measured transfer functions. A significant nonlinear characteristic for the input voltage level existed up to approximately 30 Hz in the frequency response. The models that corresponded to an input voltage can be identified by altering the parameters of the suspension system and noting the changes; the dashed red lines represent the models. Fig. 3 shows that the characteristic of the model is consistent with the measured transfer function at each input level. The model that measured by using the white noise, set at 150 mV rms, is defined as the nominal model. The perturbed regions of these parameters are obtained by comparing the nominal model with the other models.

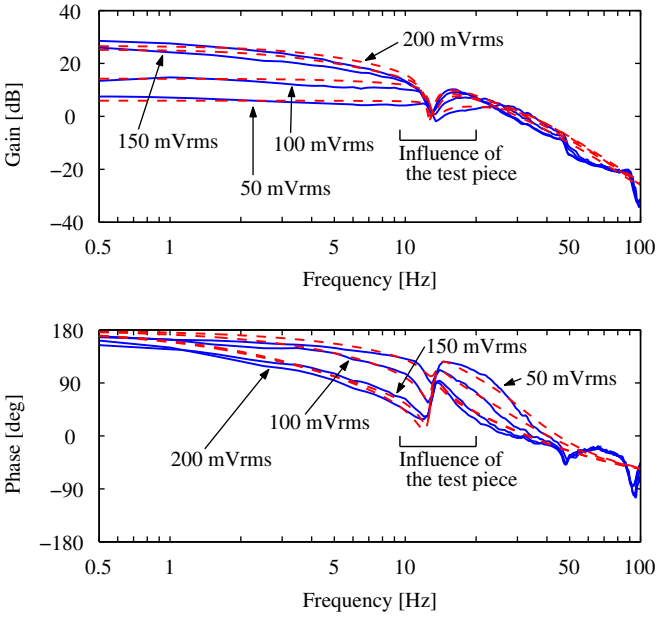

Fig. 3. Transfer function for the system with measurements of various input levels (solid blue line) and the characteristic for the model with parameter adjustments for the measured data (dashed red line). (For interpretation of the references to colour in this figure legend, the reader is referred to the web version of this article.)

Additive uncertainties caused by the influence of the specimen and parameter perturbations of the shaker are also considered. The various parameter perturbations and their perturbed ranges are shown in Table 1. In order to estimate the values of these additive model perturbations, the differences between the nominal transfer function and the perturbed transfer functions are calculated when only one parameter is changed and the others are fixed. The perturbed models in Fig. 4 are plotted by using the minimum and maximum values of each parameter. Furthermore, the influence of the difference between the nominal model and the model with the test piece is investigated. The resonant frequencies for the specimen are set at 13.2 and 12.6 Hz. The results of which shown in Fig. 4(d). The magnitude of the weighting function W_a selected to cover all the perturbations can be expressed as follows [18]:

$$W_a = \frac{2.1(s+150)}{s+30}. \tag{4}$$

In order to reduce the influence of the uncertainties that cannot be considered, the magnitude of the weighting function is assumed to increase in the high-frequency bands.

3. Design of the 2dof controller

The design of the electrodynamic shaker controller is carried out by using MATLAB.

3.1. Objectives of the control

Controllers are required to be able to precisely replicate the measured waveform, where often the main frequency components are at lower frequency bands such as a seismic wave. In addition, the uncertainties explained in Section 2 need to be taken into account; hence, the following items were set as control objectives:

- Stabilize the system even when an uncertainty exists.
- Maintain performance by replicating the reference signal accurately.

A controller is designed to maintain robust stability against the uncertainty model. Moreover, a controller needs to maintain good performance despite the uncertainty. Therefore, the controller for the proposed system is designed by μ-synthesis, which has been used in many applications, such as Ref. [18]. This system employs a 2dof controller to improve the transient response. An adaptive filter is then added in order to meet the control performance requirements and is described in the next section.

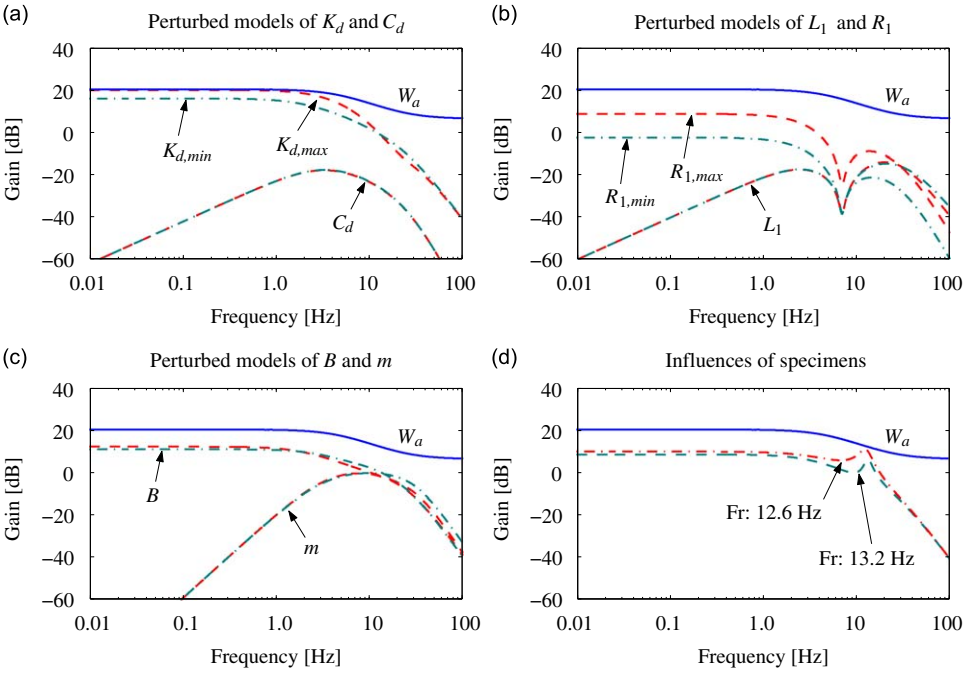

Fig. 4. Weighting function W_a (solid blue line) along with additional uncertainties: (a) stiffness coefficient K_d and damping coefficient C_d, (b) inductance L_1 and resistance R_1, (c) magnetic flux density B and armature mass m, and (d) influence of the specimen. The perturbed models derived by using the maximum values are denoted by a dashed red line in (a)–(c). The perturbed models derived by using the minimum values are denoted by a chained green line in (a)–(c). The influences of the specimen for which the resonant frequencies Fr are set at 12.6 and 13.2 Hz are denoted by a dashed green line and a chained red line, respectively, in (d). (For interpretation of the references to colour in this figure legend, the reader is referred to the web version of this article.)

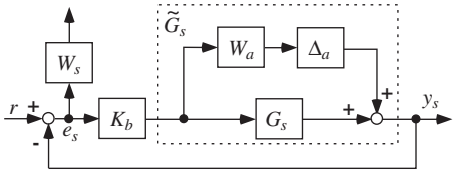

Fig. 5. Block diagram of the feedback structure with weighting functions for μ-synthesis.

3.2. μ-synthesis

In the feedback structure shown in Fig. 5, r represents the reference signal, e_s is the control error, and K_b is the feedback controller.

In order to precisely replicate the reference signal, a weighting function W_s is considered. For the precise replication of a seismic wave, the gain of the low-frequency band is required to be enlarged in order to obtain robust stability. In contrast, the influence of unconsidered uncertainties existed at higher frequencies. Furthermore, since the displacement signal is employed in the response, the signal-to-noise ratio is lower in those frequency bands. In order to avoid these problems, W_s is adjusted in the experiment by multiplying four first-order systems. On the other hand, the second-order system, where the characteristic of the high pass filter is included, is used because it contained the characteristic of the AC coupling in the amplifier. As a result, the design weight W_s is now expressed as

$$W_s = \frac{10 \cdot \alpha \cdot 0.4 \cdot 2\pi}{s + 0.4 \cdot 2\pi} \cdot \frac{0.8 \cdot 2\pi}{s + 0.8 \cdot 2\pi} \left(\frac{4 \cdot 2\pi}{s + 4 \cdot 2\pi} \right)^2 \frac{s^2}{s^2 + 0.89s + 0.39}, \tag{5}$$

where α represents the adjustment parameter, which is selected to be 1.2.

The design objective for stability and control performance is formalized as a requirement for a closed-loop transfer function with weighting functions. Therefore the generalized plant P, shown in Fig. 6, is constructed to deal with the control objectives of the μ-synthesis framework. Here, the block structure for the uncertainty Δ is defined as

$$\Delta := \{\mathrm{diag}(\Delta_a, \Delta_{perf}), \Delta_a \in \mathscr{C}^{1\times 1}, \Delta_{perf} \in \mathscr{C}^{1\times 1}\}, \tag{6}$$

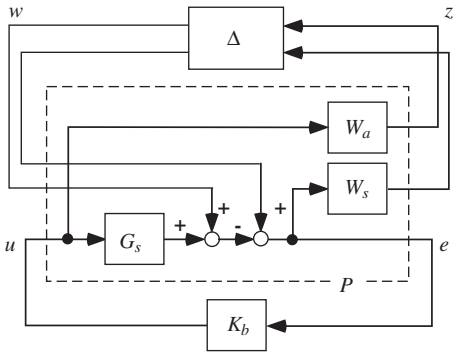

Fig. 6. Block diagram of generalized plant designed using μ-synthesis.

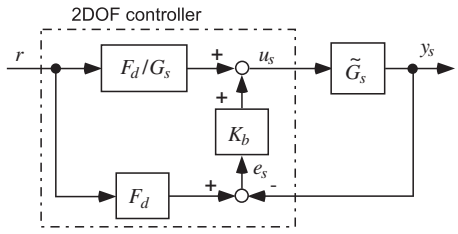

Fig. 7. Block diagram for the 2dof controller.

where $|\Delta_a| \leqslant 1$ and $|\Delta_{perf}| \leqslant 1$. Here, Δ_{perf} represents a hypothetical uncertainty block for considering a robust performance. Since the controller satisfies the robust performance condition, the D–K iteration procedure is employed. In this paper, the controller can be obtained after two iterations, and the degree of the controller is reduced from 16 to 10 states.

3.3. Construction of the 2dof controller

The 2dof controller shown in Fig. 7 is introduced to improve its transient response to the reference signal [19]. F_d and $\tilde{G}_s$ represent the reference model and the actual plant. This control system has the advantage that the transfer function $G_{y_s r}$ from the reference r to the response displacement y_s can be determined by F_d irrespective of the choice of K_b. If the nominal model was perfect, or $G_s = \tilde{G}_s$, then the transfer function becomes $G_{y_s r} = F_d$. This equation supports the assumption that the reference characteristic of the system can be determined by F_d. However, the actual plant is in general known to be imperfect and so G_s is not equal to $\tilde{G}_s$. The feedback stability is determined by K_b irrespective of F_d. In addition, when the feedback control works precisely, $G_{y_s r}$ becomes equal to F_d.

For the precise replication of a reference signal, a small phase delay characteristic at a low frequency is desirable. A low-pass Butterworth filter with a cutoff frequency of 20 Hz is applied for this purpose. F_d is set to the fifth order in order to obtain a proper F_d/G_s.

4. Adaptive filter based on the H_∞ filter

In order to compensate for the difference between the model and the actual plant, this section describes the adaptive filter adds to the proposed system.

4.1. Application to an electrodynamic shaker

In general, the plant's actual characteristic differs from that of the nominal model due to the influence of the interaction between the specimen and the nonlinear characteristic. In practice, such an influence appears in the response signal. This influence becomes particularly dominant when the frequency is beyond the frequency range of the feedback controller. Therefore, the addition of the adaptive filter to the feedforward term enables the compensation for plant perturbation through online updates. When the adaptive filter is used instead of F_d/G_s, the filter converges over a period of time and the transient response is likely to worsen. Therefore, an adaptive filter is inserted in series with the existent feedforward block as shown in Fig. 8. The transfer function $G_{y_s r}$ from reference r to the response displacement y_s is

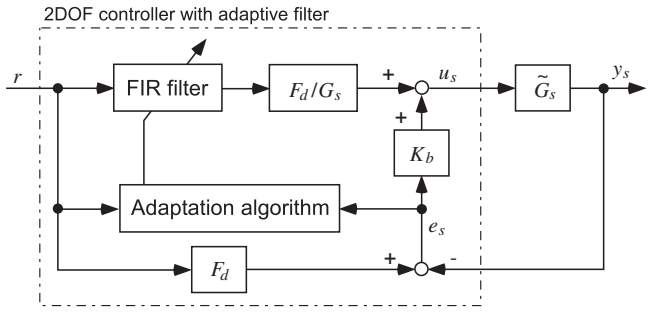

Fig. 8. Block diagram of the 2dof controller with the adaptive filter in order to improve the control performance.

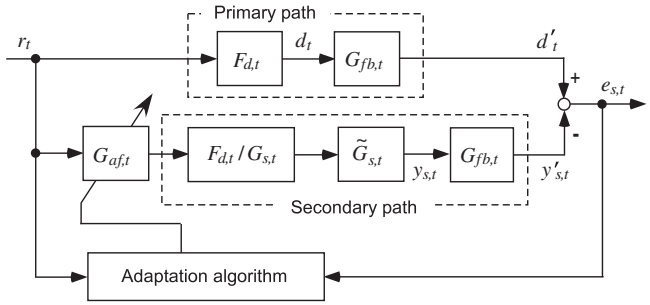

Fig. 9. Block diagram of the feedback term arrangement with the sensitivity function to consider design of the adaptive filter mainly.

given here

$$G_{y_s r} = (1 + \tilde{G}_s K_b)^{-1} \left(\tilde{G}_s K_b + \frac{\tilde{G}_s}{G_s} G_{af} \right) F_d. \tag{7}$$

Here, G_{af} denotes the characteristic of the adaptive filter. The objective of this adaptive filter is to ensure that $G_{y_s r}$ equals F_d. This way, the characteristics of the optimally adjusted adaptive filter can be given by $G_{af} = G_s/\tilde{G}_s$. The filter is structured to compensate for the difference between the nominal model and the actual plant.

It has been noted that the stability of the feedback control system after the addition of the adaptive filter should not be fully compensated. The stability analysis for this control system with the adaptive filter is certainly incomplete. However, in order to apply this adaptive method to the electrodynamic shaker experimentally, the influence of the addition of the adaptive filter is confirmed by the actual excitation experiment. This adaptive filter is typically discussed in a discrete system; the controller is designed with the continuous time system described in the previous section and discretized via the Tustin transform. The discretized parameters are indicated by the subscripts "t".

In order to clarify the description for the adaptive filter, the feedback term is arranged as shown in Fig. 9 using $G_{fb,t} = (1 + \tilde{G}_{s,t} K_{b,t})^{-1}$, where the characteristic represented the sensitivity function. Since the error signal $e_{s,t}$ is applied to the sensitivity function in Fig. 9, the level of $e_{s,t}$ was considered to be low and within the controllable frequency band of the feedback controller. Therefore, the adaptive filter only has to compensate for the difference between $\tilde{G}_{s,t}$ and $G_{s,t}$, which was beyond the controllable band of the feedback controller. On the other hand, when the controller is constituted by such blocks, the transfer function for the secondary pass from the filter output to the error signal needs to be considered. However, the uncertainty exists in the secondary path of the actual plant $\tilde{G}_{s,t}$. The estimation-based adaptive filtering (EBAF) method [16] based on the H_∞ estimation problem is then employed so that the uncertainty is explicitly considered.

4.2. Configuration of the H_∞ filtering problem

In order to employ the EBAF method, the system shown in Fig. 9 can be interpreted as an estimation problem. The objective of the adaptive filter is to generate a filter output such that the output of the secondary path $y'_{s,t}$ is similar to the output of the primary path d'_t. When the adaptive filter is adequately adjusted, the characteristic from r_t to d'_t should be equivalent to the characteristic from r_t to $y'_{s,t}$ since $y'_{s,t}$ should equal d'_t. Therefore, an approximate model of the primary path can then be constituted using the secondary path, and the system shown in Fig. 9 is then transformed into the system shown in Fig. 10. Here, the secondary path is assumed to be equivalent to the nominal model. However, because there is an uncertainty corresponding to the difference between the actual plant and the model in the secondary path, a modelling

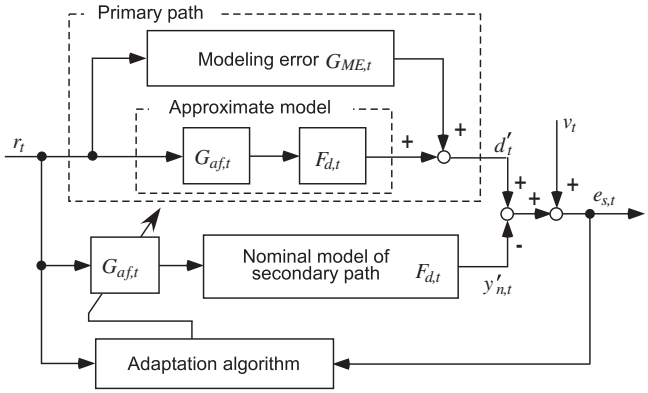

Fig. 10. Block diagram which replaces the primary path with its approximate model for reinterpretation as an estimation problem.

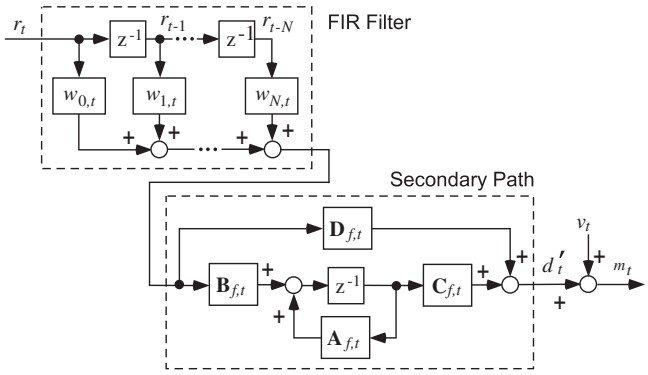

Fig. 11. Block diagram for the approximated model of the primary path.

error $G_{ME,t}$ is introduced to account for the uncertainty and expressed as

$$G_{ME,t} = (G_{fb,t}\tilde{G}_{s,t}G_{s,t}^{-1} - 1)F_{d,t}G_{af,t}. \tag{8}$$

Furthermore, Fig. 10 shows that the influence of the uncertainty is treated as the input disturbance v_t.

As stated above, the control objective of the adaptive filter is formalized as the problem that estimates the desired signal d'_t under a disturbance. The measured quantity m_t used in the estimation process is defined as the sum of the reference quantity d'_t and the disturbance v_t. However, m_t is calculated by adding the output $y'_{n,t}$ of the nominal model to the control error $e_{s,t}$ because v_t cannot be measured directly

$$m_t \equiv d'_t + v_t = e_{s,t} + y'_{n,t}. \tag{9}$$

The approximate model for the primary path is shown in Fig. 11, where $\mathbf{A}_{f,t}, \mathbf{B}_{f,t}, \mathbf{C}_{f,t}, \mathbf{D}_{f,t}$ represent the state-space matrices of the secondary path, $\mathbf{w}_t = [w_{0,t}, w_{1,t}, \ldots, w_{N,t}]^{\mathrm{T}}$ is the filter weight coefficient, and $\mathbf{x}_{f,t}$ is the state variable of the secondary path. In addition, the state variables for the overall system are set to $\mathbf{x}_t^{\mathrm{T}} = [\mathbf{w}_t^{\mathrm{T}}\mathbf{x}_{f,t}^{\mathrm{T}}]^{\mathrm{T}}$; the state-space representation of the system Γ of Fig. 11 is

$$\begin{bmatrix} \mathbf{w}_{t+1} \\ \mathbf{x}_{f,t+1} \end{bmatrix} = \begin{bmatrix} \mathbf{I}_{(N+1)\times(N+1)} & 0 \\ \mathbf{B}_{f,t}\mathbf{h}_t^{\mathrm{T}} & \mathbf{A}_{f,t} \end{bmatrix} \begin{bmatrix} \mathbf{w}_t \\ \mathbf{x}_{f,t} \end{bmatrix} := \mathbf{F}_t\mathbf{x}_t, \tag{10}$$

where $\mathbf{h}_t = [r_t, r_{t-1}, \ldots, r_{t-N}]^{\mathrm{T}}$. The measured output defined in Eq. (9) can be rewritten as

$$m_t = [\mathbf{D}_{f,t}\mathbf{h}_t^{\mathrm{T}} \;\; \mathbf{C}_{f,t}] \begin{bmatrix} \mathbf{w}_t \\ \mathbf{x}_{f,t} \end{bmatrix} + v_t := \mathbf{H}_t\mathbf{x}_t + v_t. \tag{11}$$

The estimated quantity is then defined as follows:

$$z_t = [\mathbf{L}_{1,t} \ \ \mathbf{L}_{2,t}] \begin{bmatrix} \mathbf{w}_t \\ \mathbf{x}_{f,t} \end{bmatrix} := \mathbf{L}_t \mathbf{x}_t, \tag{12}$$

where $m_t \in \mathscr{R}^{1\times 1}$, $z_t \in \mathscr{R}^{1\times 1}$, $\mathbf{x}_{f,t} \in \mathscr{R}^{N_s\times 1}$, and $\mathbf{w}_t \in \mathscr{R}^{(N+1)\times 1}$. The $\mathbf{L}_t$ is the matrix for the estimation and is determined by selecting the desired quantity to be estimated. $\mathbf{F}_t$ is assumed to not always non-singular.

4.3. Computing algorithm for the H_∞ filtering problem

In the system Γ, for a given $\gamma > 0$, the H_∞ filtering problem is formalized as finding an estimator $\hat{z}_t = \mathscr{F}(m_{t_0}, \ldots, m_{t_1})$ such that the following relation is satisfied:

$$\sup_{\nu_t, \mathbf{x}_{t_0}} \frac{\sum_{t=t_0}^{t_1-1} \|z_t - \hat{z}_t\|^2}{\mathbf{x}_{t_0}^{\mathrm{T}} \boldsymbol{\Pi}_0^{-1} \mathbf{x}_{t_0} + \sum_{t=t_0}^{t_1-1} \|\nu_t\|^2} < \gamma^2, \tag{13}$$

where Γ is defined in the finite horizon $[t_0, t_1]$ and $\sum_{t=t_0}^{t_1} \|\nu_t\|^2 < \infty$, and $\boldsymbol{\Pi}_0 > 0$ is the weighting matrix for $\mathbf{x}_{t_0}$.

In order to solve the H_∞ filtering problem, the following minimax problem is considered and an existence condition for a solution is introduced. The inequality Eq. (13) is arranged as the following cost function:

$$\tilde{J}(\hat{z}, m, \mathbf{x}_{t_0}; t_0, \tau) := \sum_{t=t_0}^{\tau-1} \|z_t - \hat{z}_t\|^2 - \gamma^2 \left(\mathbf{x}_{t_0}^{\mathrm{T}} \boldsymbol{\Pi}_0^{-1} \mathbf{x}_{t_0} + \sum_{t=t_0}^{\tau-1} \|m_t - \mathbf{H}_t \mathbf{x}_t\|^2 \right), \tag{14}$$

where τ is a fixed value in $[t_0, t_1]$ and $\{m_t : t_0 \leqslant t \leqslant \tau\}$ is a fixed value. The minimax problem is considered as follows:

$$\min_{\hat{z}} \max_{\mathbf{x}_{t_0}} \tilde{J}(\hat{z}, m, \mathbf{x}_{t_0}; t_0, \tau). \tag{15}$$

With regard to this minimax problem, the time-updating H_∞ filtering algorithm given by Refs. [20,21] is employed. One of the computing algorithms for the H_∞ filter of the system Γ is given by

$$\hat{z}_t = \mathbf{L_t}\hat{\mathbf{x}}_t + \mathbf{L}_t \mathbf{M}_t \mathbf{H}_t^{\mathrm{T}} (I + \mathbf{H}_t \mathbf{M}_t \mathbf{H}_t^{\mathrm{T}})^{-1} (m_t - \mathbf{H}_t \hat{\mathbf{x}}_t), \tag{16}$$

where $t_0 \leqslant t \leqslant t_1$, and $\hat{x}_t$ is given by

$$\hat{\mathbf{x}}_{t+1} = \mathbf{F}_t \hat{\mathbf{x}}_t + \mathbf{F}_t \mathbf{M}_t \mathbf{H}_t^{\mathrm{T}} (I + \mathbf{H}_t \mathbf{M}_t \mathbf{H}_t^{\mathrm{T}})^{-1} (m_t - \mathbf{H}_t \hat{\mathbf{x}}_t), \tag{17}$$

$$\hat{\mathbf{x}}_{t_0} = \mathbf{0}. \tag{18}$$

$\mathbf{M}_t$ is calculated by the time update algorithm as follows:

$$\mathbf{M}_{t+1} = \mathbf{F}_t \boldsymbol{\Sigma}_t \mathbf{F}_t^{\mathrm{T}}, \tag{19}$$

$$\boldsymbol{\Sigma}_t^{-1} = \mathbf{M}_t^{-1} + \mathbf{H}_t^{\mathrm{T}} \mathbf{H}_t - \gamma^{-2} \mathbf{L}_t^{\mathrm{T}} \mathbf{L}_t, \tag{20}$$

$$\mathbf{M}_{t_0} = \boldsymbol{\Pi}_0, \tag{21}$$

where the discrete-time Riccati equation is required to have the solution $\boldsymbol{\Sigma}_t$ for the positive matrix in the finite horizon $[t_0, \tau]$.

5. Excitation experiment

In this section, the control performance is confirmed experimentally using the controller designed above. The experiment is performed by the system described in Section 2.

5.1. Settings for the excitation experiment

In order to use a controller with a processing board, the controller is discretized via the Tustin transform at a sampling frequency of 512 Hz. This experiment is performed by excitation using a measured displacement waveform data as the reference signal. This experiment is performed by excitation using a measured displacement waveform data as the reference signal, which is shown in Fig. 12. The frequency components of this reference signal are dominant at a low frequency, where the uncertainty for friction exists as shown in Fig. 3. Therefore, in order to improve the control performance, the influence of friction needs to be compensated for. The control performance is evaluated based upon the transient response during excitation. The experiment is executed by changing the level of the reference waveform to investigate the influence of variations in the friction force. Because the nonlinear characteristic shown in Fig. 3 exists, the

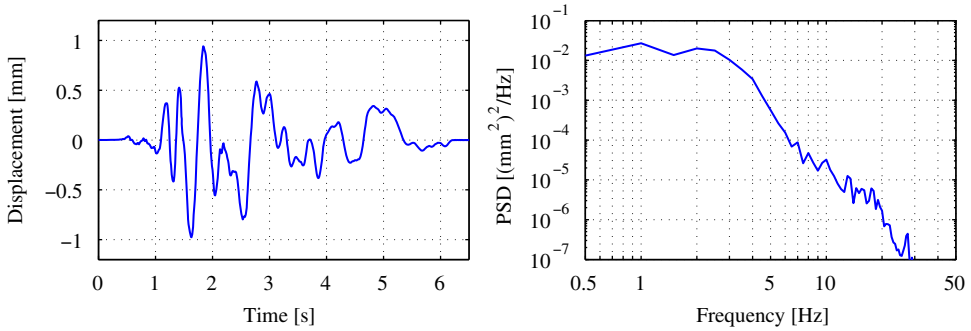

Fig. 12. Transient response and frequency response of the reference signal.

characteristic of the secondary path is changed for the level of the reference waveform. Therefore, the different uncertainties appear in the secondary path, and which allows the control performance for the influence to be estimated.

The secondary path in Fig. 11 is set as the reference model $F_{d,t}$. The matrix $\mathbf{L}_t$ is chosen as $\mathbf{L}_t = \mathbf{H}_t$ for the estimation problem such that the estimation quantity z_t is equivalent to d'_t. The length of the FIR filter is set at 16 to reduce the calculations required. Due to the short filter length, it appears that the errors in the adaptive filter cannot be fully converged. γ is kept at $\gamma = 1$. Based upon these set parameters, the amount of calculation is reduced for Eqs. (19)–(21). The initial value $\mathbf{\Pi}_0$ for Eq. (21) is chosen to reduce the error to within a range that satisfies both the stability and performance requirements. For comparison with a conventional method, a filtered-X LMS method is used in the experiment. The filter length is selected as 16 to match the EBAF method, and a convergence factor is obtained in the same manner as the choice of $\mathbf{\Pi}_0$.

5.2. Conventional method

In order to compare a conventional method with the proposal method, a conventional open-loop control with iterative excitation is used. The iteration process of this conventional method is summarized as follows:

Step 1. The first drive is calculated from the measurement transfer function.
Step 2. The excitation is performed, and an error signal is obtained.
Step 3. The next drive signal is computed from the previous drive and error signal.
Step 4. Repeat from *Step 2*.

Here, the drive signal denotes the output from the controller to the amplifier.

First, the conventional control is considered. The control results using the first drive signal are shown in Fig. 13(a) and those after the third iteration are shown in Fig. 13(b). The left figures represent the reference and response signals, denoted by the dashed red and solid blue lines, respectively. The right figures represent the error signal. Also, the rms error (= rms value of the error signal / rms value of the reference signal × 100%) and the peak error are shown in the figures. Due to the influence of the nonlinear perturbation of the system, it is difficult for the control using the first drive signal to yield good results and the tracking error is enlarged, as shown in Fig. 13(a). Since the drive signal is updated by the third iterative compensation, waveform replication can yield a good performance when compared with using the first drive signal.

5.3. Experimental results for the proposed method

The results obtain using reference waveforms that have different levels are shown in Figs. 14–16. The (a) sections of Figs. 14–16 show the results for when the peak value of the reference waveform of magnitude is set to 0.6 mm and the (b) sections similarly show the results for waveforms with magnitudes of 1 mm. As in Fig. 13, the left figures represent the reference and response signals, and the right figures represent the error signal.

Fig. 14 shows in the results of the 2dof controller without the adaptive filter that the response waveform differs significantly from the reference waveform. Since the trend of the transient response varies with the level of the reference, the influence of friction is confirmed. In these results, even though such an uncertainty exists, the control is stable. However, since the nominal model differs from the actual plant, a good performance is not obtained. The experimental results obtain by the filtered-X LMS method under the same condition are shown in Fig. 15. By comparing these with the results for the 2dof controller, the rms error is improved when the peak value of the reference waveform is 0.6 mm; however, the rms error for a 1 mm magnitude increased slightly.

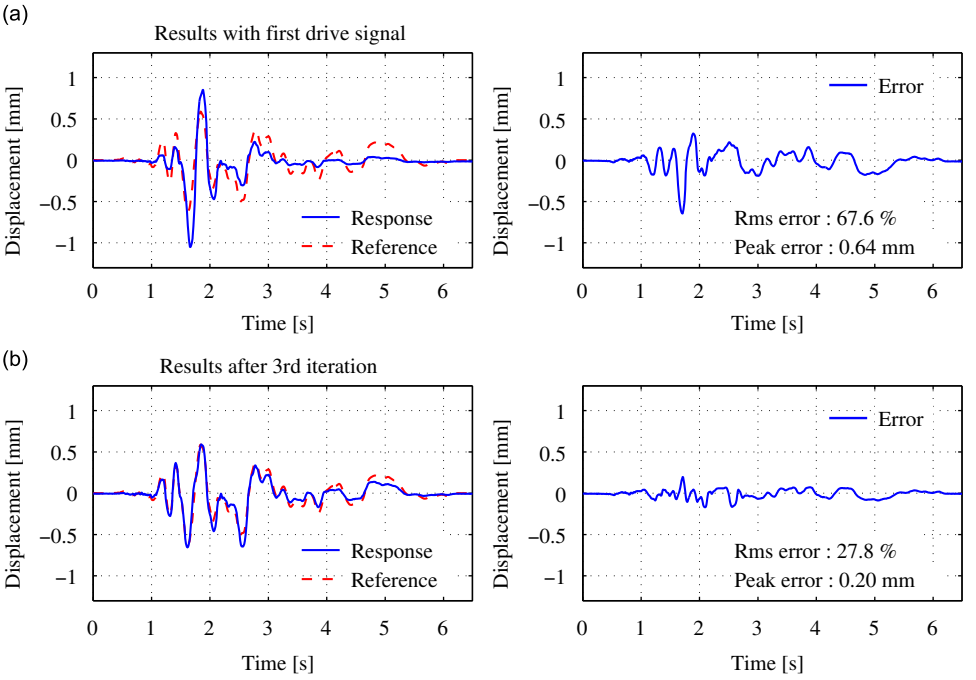

Fig. 13. Excitation results with the conventional controller when the peak value of the reference is set at 0.6 mm: (a) with the first drive signal; (b) after the third iteration. The figures on the left side show the response (solid blue line) and reference signals (dashed red line), and the figures on the right side show the error signals (solid blue line). (For interpretation of the references to colour in this figure legend, the reader is referred to the web version of this article.)

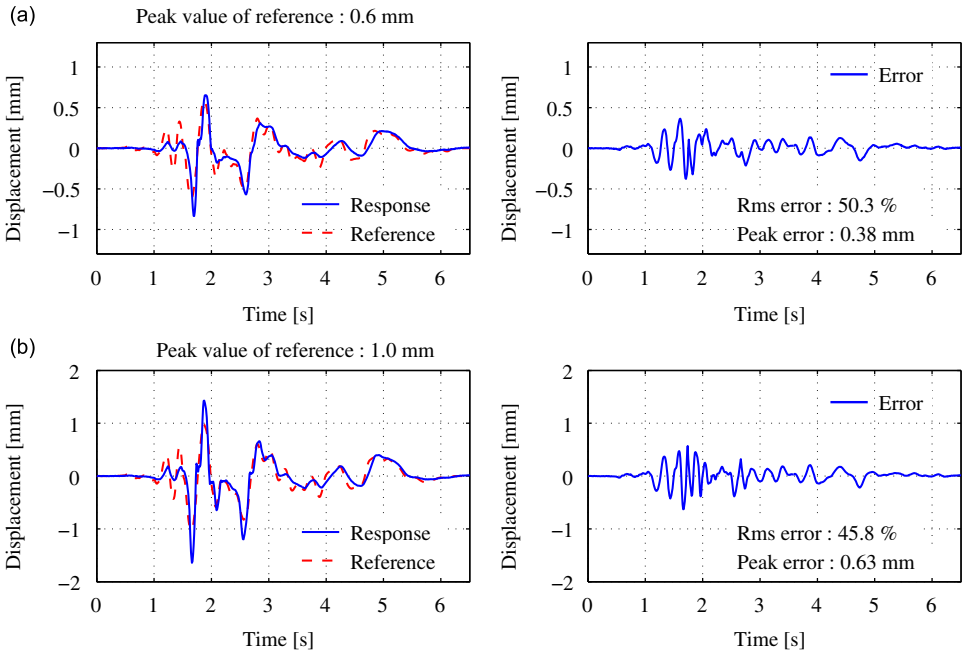

Fig. 14. Excitation results for the 2dof controller without the adaptive filter: (a) the peak value is set at 0.6 mm; (b) the peak value is set at 1.0 mm. The figures on the left side show the response (solid blue line) and reference signals (dashed red line), and the figures on the right side show the error signals (solid blue line). (For interpretation of the references to colour in this figure legend, the reader is referred to the web version of this article.)

Fig. 16 shows the experimental results obtained using the EBAF method. By comparing them with the results shown in Figs. 14 and 15, the tracking ability to the reference waveform is shown to yield a good performance when the EBAF method is applied, and the rms error decreases approximately 13% compared to the 2dof controller irrespective of the level of the

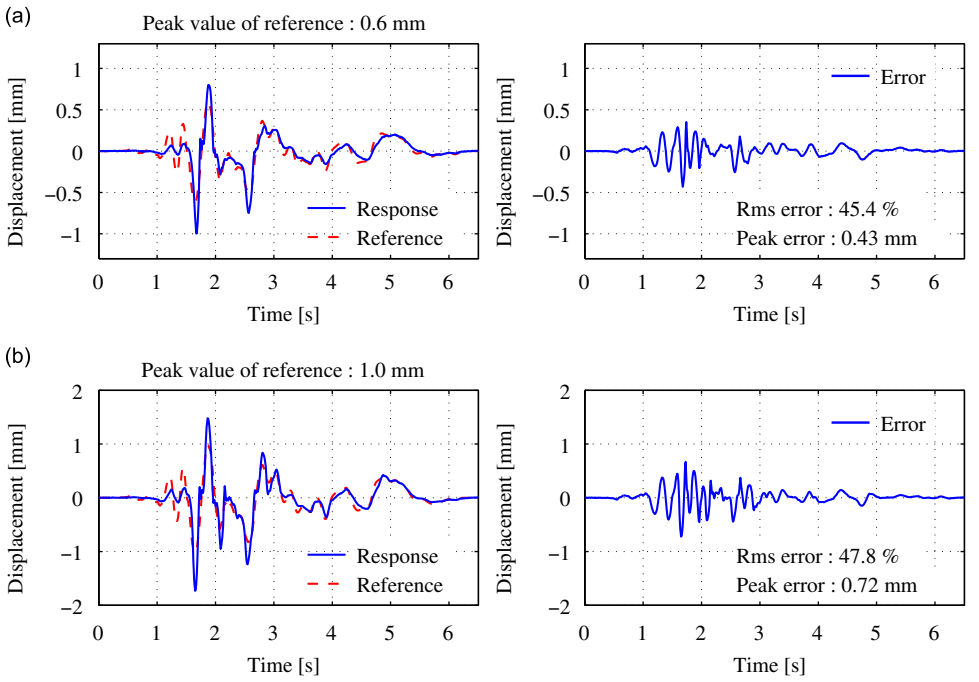

Fig. 15. Excitation results for the 2dof controller with the filtered-X LMS: (a) the peak value is set at 0.6 mm; (b) the peak value is set at 1.0 mm. The figures on the left side show the response (solid blue line) and reference signals (dashed red line), and the figures on the right side show the error signals (solid blue line). (For interpretation of the references to colour in this figure legend, the reader is referred to the web version of this article.)

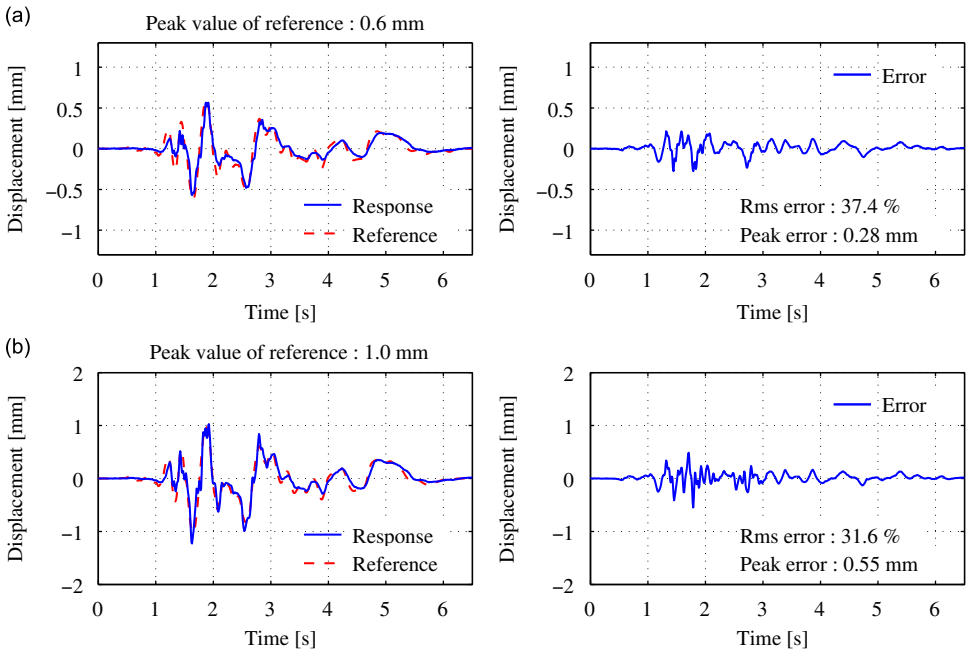

Fig. 16. Excitation results for the 2dof controller with the EBAF method: (a) the peak value is set at 0.6 mm; (b) the peak value is set at 1.0 mm. The figures on the left side show the response (solid blue line) and reference signals (dashed red line), and the figures on the right side show the error signals (solid blue line). (For interpretation of the references to colour in this figure legend, the reader is referred to the web version of this article.)

reference signal. The maximum error also improves compared with the other control results. For the time period of 1.5–2 s, where the reference signal varies widely, the response signal in other control results overshot the reference, while the response of the EBAF method is specifically suppressed. It should be noted that a specimen is not subjected to a bigger load than that assumed during the vibration test. This way, superior control results are obtained.

6. Conclusion

In this paper, a robust controller using an adaptive filter based on the H_∞ filtering problem was used for an electrodynamic shaker control, and excitation experiments were performed to evaluate the control performance. It was assumed that the conventional open-loop method using iterative compensation by repetitive excitations could not be employed, and the proposed controller was accordingly designed for this condition. A more robust controller was developed by adding the adaptive filter from the EBAF method to the 2dof controller using μ-synthesis. From the good experimental results for the nonlinear plant, the controller was shown to be useful under the assumed conditions. Although a reduction in the computational complexity is required, in comparison with a conventional method, the proposed controller should be especially effective when dealing with uncertainties.

References

[1] K. Konagai, R. Ahsan, Simulation of nonlinear soil-structure interaction on a shaking table, *Journal of Earthquake Engineering* 6 (1) (2002) 31–51.
[2] A.M. Karshenas, M.W. Dunnigan, B.W. Williams, Adaptive inverse control algorithm for shock testing, *IEE Proceedings of Control Theory and Applications* 147 (3) (2000) 267–276.
[3] C.M. Liaw, W.C. Yu, T.H. Chen, Random vibration test control of inverter-fed electrodynamic shaker, *IEEE Transactions on Industrial Electronics* 49 (3) (2002) 587–594.
[4] D. Stoten, E. Gomez, Recent application results of adaptive control on multi-axis shaking tables, *Proceedings of the Sixth SECED International Conference, Seismic Design Practice into the Next Century*, 1998, pp. 381–387.
[5] Y. Dozono, T. Horiuchi, T. Konno, H. Katsumata, Shaking-table control by real-time compensation of the reaction force caused by a nonlinear specimen, *Transactions of the ASME Journal of Pressure Vessel Technology* 126 (1) (2004) 122–127.
[6] C. Lauwerys, J. Swevers, P. Sas, Robust linear control of an active suspension on a quarter car test-rig, *Control Engineering Practice* 13 (2005) 577–586.
[7] R. de Callafon, R. Nagamune, R. Horowitz, Robust dynamic modeling and control of dual-stage actuators, *IEEE Transactions on Magnetics* 42 (2) (2006) 247–254.
[8] J.A. Mynderse, W.C. Messner, G.T.C. Chiu, H_∞ loopshaping control of a steering wheel vibration simulator using complex lead filter, *Proceedings of the European Control Conference 2007*, Kos, Greece, 2007, pp. 1406–1413.
[9] S. Adachi, H. Sano, Active noise control system for automobiles based on adaptive and robust control, *Proceedings of the 1998 IEEE International Conference on Control Applications*, 1998, pp. 1125–1129.
[10] J. Yang, Y. Suematsu, Z. Kang, Two-degree-of-freedom controller to reduce the vibration of vehicle engine-body system, *IEEE Transactions on Control Systems Technology* 9 (2) (2001) 295–304.
[11] Y. Uchiyama, M. Fujita, Application of two-degree-of-freedom control to multi-axis electro-dynamic shaking system using μ—synthesis and adaptive filter, *Proceedings of the Sixth International Conference on Motion and Vibration Control*, Saitama, Japan, 2002, pp. 253–258.
[12] C. Bao, P. Sas, H. Brussel, Adaptive active control of noise in 3-d reverberant enclosures, *Journal of Sound and Vibration* 161 (1993) 501–514.
[13] Q.-Z. Zhang, W.-S. Gan, A model predictive algorithm for active noise control with online secondary path modelling, *Journal of Sound and Vibration* 270 (2004) 1056–1066.
[14] D. Zhou, V. DeBrunner, A new active noise control algorithm that requires no secondary path identification based on the SPR property, *IEEE Transactions on Signal Processing* 55 (5) (2007) 1719–1729.
[15] T. Kouno, H. Ohmori, A. Sano, New direct adaptive active noise control algorithms in case of uncertain secondary path dynamics, *Proceedings of the American Control Conference*, 2002, pp. 1767–1772.
[16] B. Sayyarrodsari, J. How, B. Hassibi, A. Carrier, Estimation-based synthesis of H_∞-optimal adaptive fir filters for filtered-LMS problems, *IEEE Transactions on Signal Processing* 49 (1) (2001) 164–178.
[17] A. Maleki-Tehrani, B. Sayyarrodsari, B. Hassibi, J. How, J. Cioffi, Estimation-based synthesis of H_∞-optimal adaptive equalizers over wireless channels, *Proceedings of IEEE GLOBECOM '99*, vol. 1a, 1999, pp. 457–461.
[18] M. Fujita, T. Namerikawa, F. Matsumura, K. Uchida, μ-synthesis of an electromagnetic suspension system, *IEEE Transactions on Automatic Control* 40 (3) (1995) 530–536.
[19] T. Sugie, T. Yoshikawa, General solution of robust tracking problem in two-degree-of-freedom control systems, *IEEE Transactions on Automatic Control* 31 (6) (1986) 552–554.
[20] M. Fujita, A. Maruyama, T. Taniguchi, K. Uchida, Finite horizon discrete-time H_∞ filter with application to an active vision system, *Proceedings of the 32nd IEEE Conference on Decision and Control*, 1993, pp. 2194–2196.
[21] A. Kawabata, M. Fujita, Design of an H_∞ filter-based robust visual servoing system, *Control Engineering Practice* 6 (1998) 219–225.